Analysis of non-data-aided carrier frequency recovery with Luise–Reggiannini estimators applied to *M*-PSK schemes

W. Gappmair

Abstract: Luise and Reggiannini introduced a data-aided feedforward estimator for carrier frequency recovery in an all-digital receiver. For *M*-PSK as a modulation scheme, the concept is easily extended to the non-data-aided case. In this context, a closed-form solution for computation of the jitter variance is provided, which agrees with the simulation results for medium-to-high SNR values and frequency offsets representing a smaller fraction of the operational range. In the sequel, the analytical result is used for comparison purposes and parameter optimisation.

1 Introduction

Luise and Reggiannini (L&R) introduced a data-aided (DA) feedforward estimator for carrier frequency recovery in an all-digital receiver [1]. Derived from the maximum-likelihood principle, the algorithm is particularly attractive for time-division multiple access (TDMA) systems, where rapid and effective acquisition procedures are required [2]. In practice, this is achieved through a predefined sequence of symbols (preamble, unique word).

For *M*-ary phase-shift keying (*M*-PSK) as a modulation scheme, the L&R concept is easily extended to the non-data-aided (NDA) case using an *M*th power nonlinearity [3, 4]. Mainly for continuous transmission of data, as it is typical for DVB environments [5], NDA recovery of the carrier frequency is highly welcome since the accuracy of the estimate may be increased arbitrarily via the selected observation length. For DA recovery, in contrast, larger preambles, contributing to the overall redundancy, would be necessary.

With DA L&R estimators, the jitter variance is known in closed-form [1]. In this respect, however, little is available from the open literature for NDA variants applied to *M*-PSK. Instead, simulation results are frequently compared to the so-called Cramer–Rao lower bound as the theoretical performance limit [2, 6, 7]. Nevertheless, the optimisation of the design parameters, forming part of NDA L&R estimators as will be carried out in the following, requires a considerable amount of simulation work if no analytical solution is at hand. Therefore, an appropriate relationship is to be developed subsequently.

IEE Proceedings online no. 20045212

doi:10.1049/ip-com:20045212

Paper first received 7th August and in revised form 27th November 2004

The author is with the Institute of Communication Networks and Satellite Communications, Graz University of Technology, Inffeldgasse 12, 8010 Graz, Austria

E-mail: gappmair@inw.tugraz.at

2 Equivalent baseband model

Throughout this paper, it is assumed that perfect symbol timing has been achieved and that the independent and identically distributed (i.i.d.) *M*-PSK symbols are solely distorted by additive white Gaussian noise (AWGN). In the complex baseband model with timing index k, let the symbols be denoted by c_k and normalised to the expectation $E[|c_k|^2] = 1$. Further, let the samples r_k at the output of the matched filter be rotated by $2\pi kvT + \theta$, i.e.

$$r_k = c_k e^{j(2\pi kvT+\theta)} + n_k \tag{1}$$

where $\theta \in [-\pi, \pi)$ is the carrier phase and v represents the carrier frequency offset. Real and imaginary part of the zero-mean complex AWGN samples $n_k = n_{k,c} + jn_{k,s}$ are assumed to be independent, each with the same (normalised) variance $1/(2\gamma_s)$, where $\gamma_s = E_s/N_0$ is defined as the signal-to-noise ratio (SNR) per symbol.

It is to be noticed that the signal model holds only true for rather limited values of v (in general, of the order of a few per cent of the symbol rate $1/T$), because r_k does not contain the mismatch between the incoming signal and the receiver filter due to frequency errors (i.e. intersymbol interferences and reduction of the available signal energy).

3 Estimator characteristic

Based on the maximum-likelihood principle, Luise and Reggiannini developed a powerful feedforward estimator for DA frequency recovery [1]. As already mentioned in the introductory section, the concept is easily modified for NDA recovery of *M*-PSK modulated signals [3, 4]. In this case, the estimate $\hat{v}$, normalised to the symbol period T, is given by

$$\hat{v}T = \frac{1}{\pi(K+1)M} \arg\left\{\sum_{k=1}^{K} R_k\right\} \tag{2}$$

where R_k is the autocorrelation of the sequence $\{r_0, r_1, r_2, \ldots, r_{L-1}\}$ defined as

$$R_k = \frac{1}{L-k} \sum_{l=k}^{L-1} |r_l r_{l-k}|^{\mu} e^{jM[\arg(r_l)-\arg(r_{l-k})]} \tag{3}$$

L denotes the estimator length in symbols and K, $0<K<L$, as well as μ, $0 \le \mu \le M$, are design parameters discussed later in more detail. Note that $\mu = M$ is nothing else than the Mth power nonlinearity applied to r_k, i.e. r_k^M, in order to remove the modulation of the symbol phase. The generalised approach in (3) is motivated by the algorithm of Viterbi and Viterbi, originally suggested for feedforward synchronisation of the carrier phase [8].

For further analysis, it makes sense to employ polar coordinates for the representation of the received samples r_k. Hence, if $c_k = e^{j2\pi i/M}$, $i = 0, 1, \ldots, M-1$, then (1) can be rewritten as

$$r_k = \rho_k e^{j(\delta_k + 2\pi k v T + \theta + \varphi_k)} \tag{4}$$

where $\rho_k = |r_k|$, $\delta_k = \arg(c_k) = 2\pi i/M$ and φ_k is the angular jitter introduced by n_k.

The operational range of (2) is limited by $\pm 1/[(K+1)M]$ since $|\arg\{\cdot\}| \le \pi$. Moreover, by taking into account that $E[\arg(x)] \approx \arg(E[x])$, which holds true for small deviations of x from its mean value, the estimate (2) exhibits no bias, (i.e. $E[\hat{v}T] = vT$). This is verified by insertion of (4) into (3); in the sequel, if the samples r_l and r_{l-k} are assumed to be independent, the expected operation $E[R_k]$ develops according to

$$\begin{aligned} &E\left[|r_l r_{l-k}|^\mu e^{jM[\arg(r_l)-\arg(r_{l-k})]}\right] \\ &= \left[Q^2(M,\mu,\gamma_s) + P^2(M,\mu,\gamma_s)\right] e^{j2\pi k M v T} \end{aligned} \tag{5}$$

The definitions $Q(M,\mu,\gamma_s) = E[\rho_k^\mu \cos M(\varphi_k + \delta_k)]$ and $P(M,\mu,\gamma_s) = E[\rho_k^\mu \sin M(\varphi_k + \delta_k)]$ are derived in the Appendix, where it is shown that $P(\cdot) = 0$. Combining (2) and (5) provides finally

$$\begin{aligned} E[\hat{v}T] = &\frac{1}{\pi(K+1)M} \\ &\times \arg\left\{ Q^2(M,\mu,\gamma_s) \frac{\sin \pi K M v T}{\sin \pi M v T} e^{j\pi(K+1)MvT} \right\} = vT \end{aligned} \tag{6}$$

In Fig. 1, the relationship is checked for 4-PSK ($L = 128$, $K = 16$, $\mu = 0$, $\gamma_s = 8$ dB) as well as 8-PSK ($L = 256$, $K = 16$, $\mu = 2$, $\gamma_s = 15$ dB). In both cases, the limited capture range can easily be observed, i.e. $|vT| < 1/[(K+1)M] = 0.015$ and 0.007, respectively. Perfect recovery of the carrier frequency with $E[\hat{v}T] = vT$ is indicated by a dashed line (throughout this paper all analytical results are visualised as lines with different style, whereas all simulation results are shown as markers with different shape).

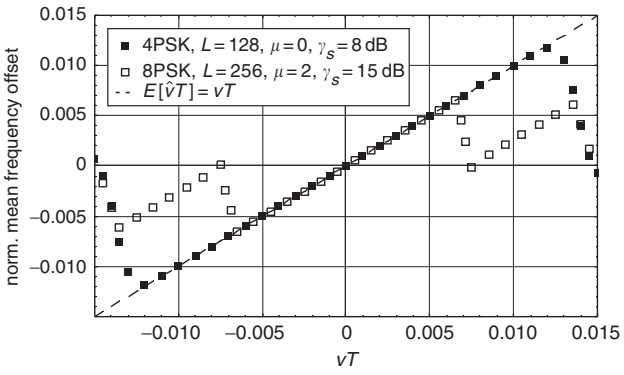

Fig. 1 *Estimator characteristic ($K = 16$)*

4 Jitter variance

The second important performance parameter, apart from the estimator characteristic, is the variance of the frequency error (jitter) $\hat{v} - v$, henceforth normalised to the symbol period T and as such denoted by σ_v^2. In digital receivers, the latter determines the residual frequency offset a device for carrier phase recovery has to cope with. In this context, an analytical relationship for σ_v^2 could be helpful in order to optimise the NDA L&R estimator, in particular with respect to μ and K. To this end, $\lambda = \arg\{\exp[j\pi(K+1)M(\hat{v}T - vT)]\}$ is introduced which provides immediately

$$\sigma_v^2 = E[(\hat{v}T - vT)^2] = \frac{1}{[\pi(K+1)M]^2} E[\lambda^2] \tag{7}$$

Replacing $\hat{v}T$ by (2) as well as assuming that $\gamma_s \gg 1$ such that $\arg\{\cdot\} \approx \mathrm{Im}\{\cdot\}/\mathrm{Re}\{\cdot\}$, λ can be approximated as

$$\begin{aligned} \lambda_N &= \left(\sum_{k=1}^{K} \frac{1}{L-k} \sum_{l=k}^{L-1} |r_l r_{l-k}|^\mu \sin[(2k-K-1)\pi M v T \right. \\ &\qquad \left. + (\varphi_l - \varphi_{l-k})M] \right) \\ \lambda &\approx \frac{}{} \\ \lambda_D &= \left(\sum_{k=1}^{K} \frac{1}{L-k} \sum_{l=k}^{L-1} |r_l r_{l-k}|^\mu \cos[(2k-K-1)\pi M v T \right. \\ &\qquad \left. + (\varphi_l - \varphi_{l-k})M] \right) \end{aligned} \tag{8}$$

If λ_N and λ_D are considered to be independent, i.e. $E[\lambda^2] \approx E[\lambda_N^2]E[1/\lambda_D^2]$, then, with Jensen's inequality [9] for u-convex functions, $E[\lambda^2]$ is lower-bounded by $E[\lambda_N^2]/E[\lambda_D^2]$. With the definitions

$$\begin{aligned} A_{c,k}(v) &= \cos[(2k-K-1)\pi M v T] \\ A_{s,k}(v) &= \sin[(2k-K-1)\pi M v T] \end{aligned} \tag{9}$$

the sine in λ_N is decomposed as $A_{c,k}(v)\sin[M(\varphi_l - \varphi_{l-k})] + A_{s,k}(v)\cos[M(\varphi_l - \varphi_{l-k})]$. After tedious but straightforward manipulations in the same way as carried out in [1], the mean square value of λ_N is provided by $E[\lambda_N^2] = 2(\Lambda_{1,c} - \Lambda_{2,c}) + \Lambda_{3,s} + \Lambda_{4,s}$, where

$$\begin{aligned} \Lambda_{1,c} = S(M,\mu,\gamma_s) &\left\{ C(M,\mu,\gamma_s) \sum_{k=1}^{K} \frac{A_{c,k}^2(v)}{L-k} \right. \\ &\left. + Q^2(M,\mu,\gamma_s) \sum_{k=1}^{K} \sum_{\substack{m=1 \\ m \ne k}}^{K} \frac{A_{c,k}(v) A_{c,m}(v) \min(L-k, L-m)}{(L-k)(L-m)} \right\} \end{aligned} \tag{10a}$$

$$\begin{aligned} \Lambda_{2,c} = &S(M,\mu,\gamma_s) Q^2(M,\mu,\gamma_s) \\ &\times \sum_{k=1}^{K} \sum_{m=1}^{K} \frac{A_{c,k}(v) A_{c,m}(v)(L-k-m)\mathrm{u}(L-k-m)}{(L-k)(L-m)} \end{aligned} \tag{10b}$$

$$\Lambda_{3,s} = Q^4(M,\mu,\gamma_s) \sum_{k=1}^{K} \sum_{m=1}^{K} A_{s,k}(v) A_{s,m}(v) \tag{10c}$$

$$\Lambda_{4,s} = S^2(M,\mu,\gamma_s) \sum_{k=1}^{K} \frac{A_{s,k}^2(v)}{L-k} \tag{10d}$$

$\mathrm{u}(\cdot)$ in (10b) denotes the unit step, i.e. $\mathrm{u}(k) = 1$ for $k = 1, 2, 3, \ldots$, and $\mathrm{u}(k) = 0$ otherwise. The expressions $C(M,\mu,\gamma_s)$ and $S(M,\mu,\gamma_s)$ are given by $E[\rho_k^{2\mu}\cos^2(M\varphi_k)]$

and $E[\rho_k^{2\mu}\sin^2(M\varphi_k)]$, respectively. Employing the trigonometric identities $\cos^2(m\varphi) \equiv \frac{1}{2}[1+\cos(2m\varphi)]$ and $\sin^2(m\varphi) \equiv \frac{1}{2}[1-\cos(2m\varphi)]$ as well as the definition of $Q(M,\mu,\gamma_s)$ given in the Appendix, i.e. $Q(M,\mu,\gamma_s) = E[\rho_k^{\mu}\cos(M\varphi_k)]$, $C(\cdot)$ and $S(\cdot)$ can be summarised as

$$\begin{aligned} C(M,\mu,\gamma_s) &= \frac{1}{2}\{Q(0,\,2\mu,\gamma_s) + Q(2M,\,2\mu,\gamma_s)\} \\ S(M,\mu,\gamma_s) &= \frac{1}{2}\{Q(0,\,2\mu,\gamma_s) - Q(2M,\,2\mu,\gamma_s)\} \end{aligned} \tag{11}$$

On the other hand, the cosine function in the denominator of (8) is simply decomposed as $A_{c,k}(v)\cos[M(\varphi_l-\varphi_{l-k})] - A_{s,k}(v)\sin[M(\varphi_l-\varphi_{l-k})]$, with $A_{c,k}(v)$ and $A_{s,k}(v)$ defined in (9). Compared to λ_N, $A_{c,k}(v)$ and $A_{s,k}(v)$ have changed their roles such that $E[\lambda_D^2]$ can be computed via (10), too, if the subscripts c and s are switched, i.e. $E[\lambda_D^2] = 2(\Lambda_{1,s}-\Lambda_{2,s}) + \Lambda_{3,c} + \Lambda_{4,c}$. Therefore, putting all pieces together,

$$\sigma_v^2 \approx \frac{1}{[\pi(K+1)M]^2}\frac{2(\Lambda_{1,c}-\Lambda_{2,c}) + \Lambda_{3,s} + \Lambda_{4,s}}{2(\Lambda_{1,s}-\Lambda_{2,s}) + \Lambda_{3,c} + \Lambda_{4,c}} \tag{12}$$

Figure 2 depicts the variance for 4-PSK ($L=128$, $\mu\in\{0,4\}$) and 8-PSK ($L=256$, $\mu\in\{2,8\}$) as a function of $\gamma_s = E_s/N_0$, $K=16$ and $v=0$. Already for medium SNRs, i.e. values in the transition range between flat top and asymptotic behaviour, the analysis agrees with the simulation results. If $\gamma_s \to 0$, the jitter variance begins to flatten since $\arg\{\cdot\}$ in (2) becomes more and more uniformly distributed between $\pm\pi$; therefore, $\sigma_v^2 \to \sigma_{v,0}^2 = 1/\{3[(K+1)M]^2\}$, which is also confirmed by the simulation results in Fig. 2. On the other hand, as soon as $\gamma_s \to 0$, $Q(M,\mu,\gamma_s) \to 0$ and $C(M,\mu,\gamma_s) = S(M,\mu,\gamma_s)$. Using these approximations in (10), σ_v^2 approaches $\sigma_{v,1}^2 = 2/[\pi(K+1)M]^2$. It is easily verified that $\sigma_{v,0}^2/\sigma_{v,1}^2$ yields $\pi^2/6 = 1.645$, which can be seen in Fig. 2 as well. If $\gamma_s \gg 1$, however, $Q(M,\mu,\gamma_s) \to 1 - M^2/(4\gamma_s)$ (see the Appendix) such that $C(M,\mu,\gamma_s) \to 1$ and $S(M,\mu,\gamma_s) \to M^2/(2\gamma_s)$. After some algebra, (12) converges to

$$\sigma_{\mathrm{DA}}^2 = \frac{1}{\gamma_s[\pi(K+1)K]^2} \times \left(\sum_{k=1}^{K}\sum_{m=1}^{K}\frac{\min(L-k,L-m) - (L-k-m)\mathrm{u}(L-k-m)}{(L-k)(L-m)}\right) \tag{13}$$

which is exactly the result for DA recovery obtained by Luise and Reggiannini in their original paper [1]. The relationship is visualised in Fig. 2 for comparison purposes (dotted lines). Hence, it is verified that the jitter of the NDA estimate (2) approaches asymptotically the performance of the corresponding DA algorithm. Note also that the jitter variance can never be located beyond a theoretical limit [2, 6, 7], the so-called modified Cramer–Rao lower bound provided by

$$\mathrm{MCRLB} = \frac{3}{2\pi^2 L(L^2-1)\gamma_s} \tag{14}$$

By detailed inspection of (10), it is obvious that the dependence of the jitter variance (12) on vT is solely caused by $A_{c,k}(v)$ and $A_{s,k}(v)$ given in (9); for $v=0$, $A_{c,k}(v)=1$ and $A_{s,k}(v)=0$ such that (10) simplifies accordingly. Figure 3 shows the evolution of (12) for 4-PSK ($L=128$, $K=16$, $\mu\in\{0,4\}$, $\gamma_s=8$ dB) as well as 8-PSK ($L=256$, $K=16$, $\mu\in\{2,8\}$, $\gamma_s=15$ dB) as a function of vT (solid lines). Figure 3 depicts also the increasing discrepancy between analytical and simulation results as soon as $|vT|$ approaches the limits of the capture range. However, for smaller offsets, say $|vT| < 1/(2KM)$, the analysis agrees with the simulation results within a factor of two.

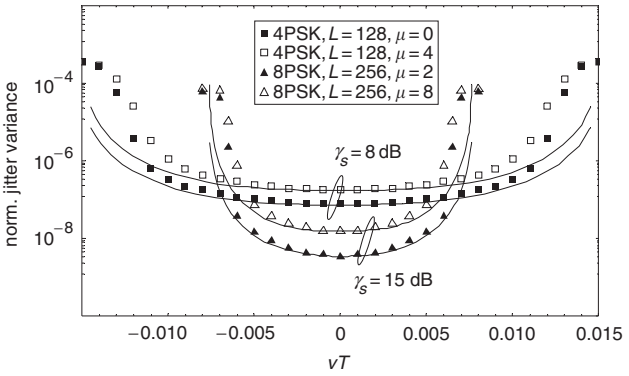

Fig. 3 *Normalised jitter variance as function of vT ($K=16$)*

5 Comparison and optimisation

For medium-to-large SNRs, (i.e. values in the transition range and beyond), and a smaller fraction of the capture range, the frequency jitter is described accurately enough by (12), exemplified in Figs. 2 and 3 for 4-PSK and 8-PSK. In the sequel, the analytical result will be used to optimise the NDA estimator with respect to the design parameters μ and K.

The autocorrelation R_k must be evaluated over $L-k$ samples, $1 \le k \le K$, $0 < K < L$, with less jitter introduced through larger values of K. Given 4-PSK ($L=128$, $\mu\in\{0,4\}$, $\gamma_s=8$ dB) and 8-PSK ($L=256$, $\mu\in\{2,8\}$, $\gamma_s=15$ dB), this is visualised in Fig. 4 showing the jitter

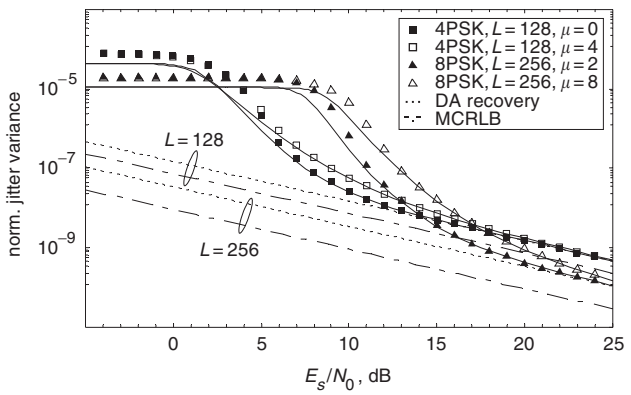

Fig. 2 *Normalised jitter variance as function of E_s/N_0 ($K=16$, $v=0$)*

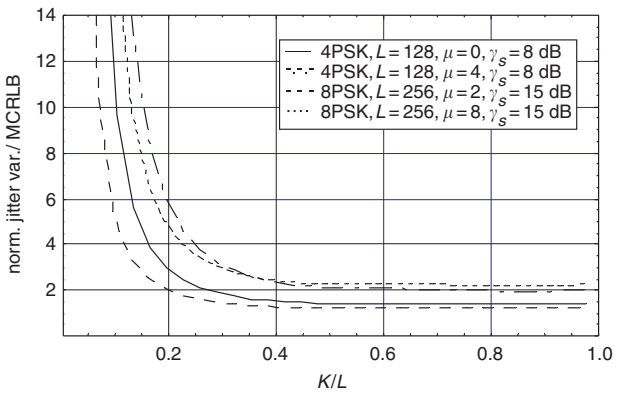

Fig. 4 *Normalised jitter variance/MCRLB as function of K/L ($v=0$)*

variance (12) normalised to MCRLB as a function of K/L. No distinct minimum can be detected. But, with $K \approx L/2$, the curves begin to flatten significantly, representing a good compromise between performance and complexity which is on the order of KL [3]. This result is also confirmed by parameter combinations other than those used in Fig. 4. It is to be noticed, however, that $K = 16$ is chosen throughout this paper since the operational range is inversely proportional to K such that the estimator may be useless in practice for higher values of K.

For 4-PSK ($L = 128$, $\gamma_s = 8$ dB) and 8-PSK ($L = 256$, $\gamma_s = 15$ dB), Fig. 5 depicts the quotient σ_v^2/MCRLB as a function of μ/M verified by simulation results ($K = 16$). With $v = 0$ (solid lines), the curves have a minimum for μ in the range between zero and one. With a moderate frequency offset (dashed lines), analytical and simulation results exhibit some discrepancy. But, even in case of larger values, as with 4-PSK and $vT = 5 \times 10^{-3}$, the simulation results are solely shifted in the vertical direction which means that the same minimum is achieved.

Given M, L, K and γ_s, the value of μ involving minimum jitter variance, henceforth denoted by μ_{opt}, requires the first derivative of (12) with respect to μ. No closed-form solution is available in this respect. Nevertheless, with Brent's algorithm [10] the problem can be tackled most efficiently. Figure 6 displays the result of the derivative procedure as a function of γ_s and $K \in \{16, L/2\}$. As a consequence, the optimum should be selected as $0 \leq \mu_{opt} \leq 1$ for medium-to-high SNR's. Given smaller values of K, $\mu_{opt} = 0$ seems to be a pragmatic solution, whereas $\mu_{opt} = 1$ might be chosen for $K \geq L/4$.

Figure 7 depicts the evolution of the symbol error rate (SER) as a function of $\gamma_s = E_s/N_0$. The simulation results are

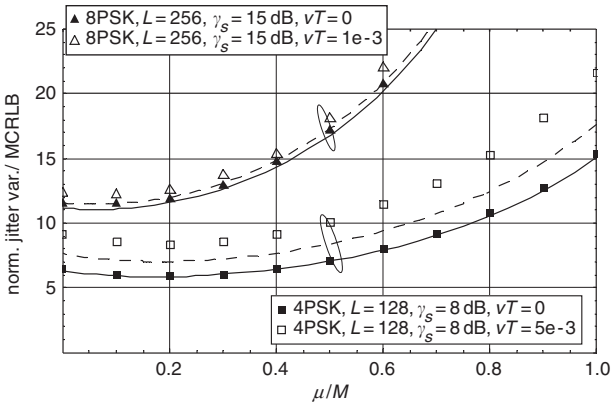

Fig. 5 *Normalised jitter variance/MCRLB as function of μ/M ($K = 16$)*

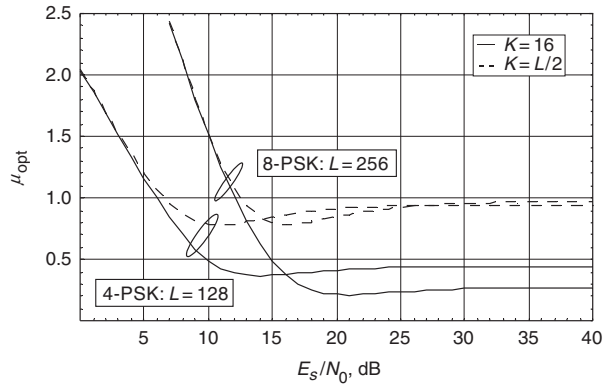

Fig. 6 *Optimised design parameter μ as function of E_s/N_0*

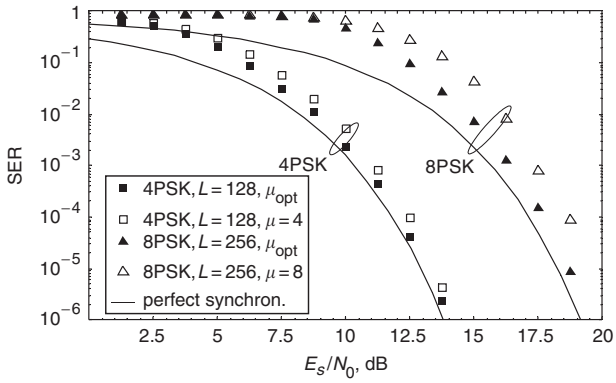

Fig. 7 *Evolution of symbol error rate ($K = 16$, $|vT| < 1/[2KM]$)*

compared to the case with perfect synchronisation (i.e. the received samples r_k are only distorted by AWGN [11]). Taking the effect of carrier frequency offsets into account, vT is assumed to be uniformly distributed between $\pm 1/(2KM)$; the simulation results are obtained with perfect symbol timing and phase recovery such that the impact of the NDA L&R estimator may be observed without side effects from other synchronisers. Using 4PSK with $L = 128$, $K = 16$ and $\mu = \mu_{opt}$ (see Fig. 6), approximately 0.2–0.5 dB are lost in the medium-to-high SNR range if compared to the ideal case; with regard to the fourth-order nonlinearity, i.e. $\mu = 4$, approximately 0.5–1.0 dB must be taken into account. On the other hand, 8PSK signals with $L = 256$, $K = 16$ and $\mu = \mu_{opt}$ show a performance loss of 0.5–1 dB in the medium-to-high SNR range, whereas 1–2 dB are wasted as soon as $\mu = 8$.

6 Concluding remarks

For DA carrier frequency recovery, Luise and Reggiannini developed a powerful feedforward estimator which can be easily modified for NDA purposes. With respect to M-PSK as modulation scheme, it has been shown that the NDA variant exhibits no bias. However, the main result is a closed-form solution of the jitter variance, which agrees with the simulation results for medium-to-high SNR values and frequency offsets representing a smaller fraction of the operational range. For SNR $\gg 1$, it is verified that the NDA jitter variance approaches asymptotically the performance of the DA estimator. In the sequel, the analytical results have been used to optimise the algorithm with regard to the involved design parameters. It turned out that $K = L/2$ is a good compromise between performance and complexity; in order to guarantee a useful operational range, however, K should be chosen small enough in practice. On the other hand, the optimum of μ is to be selected in the range $0 \leq \mu_{opt} \leq 1$ for medium-to-high SNR values; as a pragmatic solution, $\mu_{opt} = 0$ is suggested for smaller values of K, whereas $\mu_{opt} = 1$ for $K \geq L/4$.

7 Acknowledgment

Part of the work has been done in SatNEx (Satellite Communications Network of Excellence, IST NoE No. 507052) launched by the European Commission for advanced research in satellite communications within the 6th Framework Programme.

8 References

1 Luise, M., and Reggiannini, R.: 'Carrier frequency recovery in all-digital modems for burst-mode transmissions', *IEEE Trans. Commun.*, 1995, **43**, pp. 1169–1178
2 Mengali, U., and D'Andrea, A.N.: 'Synchronization techniques for digital receivers' (Plenum Press, New York, 1997)
3 Morelli, M., and Mengali, U.: 'Feedforward frequency estimation for PSK: a tutorial review', *Eur. Trans. Telecommun.*, 1998, **9**, pp. 103–116
4 Meyr, H., Moeneclaey, M., and Fechtel, S.A.: 'Digital communication receivers: synchronization, channel estimation, and signal processing' (Wiley, New York, 1998)
5 D'Amico, A.A., D'Andrea, A.N., and Reggiannini, R.: 'Efficient non-data-aided carrier and clock recovery for satellite DVB at very low signal-to-noise ratios', *IEEE J. Sel. Areas Commun.*, 2001, **19**, pp. 2320–2330
6 Rice, F., Cowley, B., Moran, B., and Rice, M.: 'Cramer–Rao bounds for QAM phase and frequency estimation', *IEEE Trans. Commun.*, 2001, **49**, pp. 1582–1591
7 Noels, N., Steendam, H., and Moeneclaey, M.: 'The true Cramer–Rao bound for carrier frequency estimation from a PSK signal', *IEEE Trans. Commun.*, 2004, **52**, pp. 834–844
8 Viterbi, A.J., and Viterbi, A.M.: 'Nonlinear estimation of PSK-modulated carrier phase with application to burst digital transmission', *IEEE Trans. Inf. Theory*, 1983, **29**, pp. 543–551
9 Viterbi, A.J., and Omura, J.K.: 'Principles of digital communication and coding' (McGraw-Hill, New York, 1979)
10 Press, W.H., Teukolsky, S.A., Vetterling, W.T., and Flannery, B.P.: 'Numerical recipes in C: the art of scientific computing' (Cambridge University Press, New York, 1994, 2nd edn.)
11 Proakis, J.G.: 'Digital communications' (McGraw-Hill, New York, 1989, 2nd edn.)
12 Abramowitz, M., and Stegun, I.A.: 'Handbook of mathematical functions' (Dover Publications, New York, 1970, 9th edn.)
13 Wolfram, S.: 'Mathematica: a system for doing mathematics by computer' (Addison-Wesley, New York, 1997, 3rd edn.)

9 Appendix

To evaluate the expected operations in Sections 3 and 4, it makes sense to express the related probability density function (PDF) in polar coordinates. Given c_k and γ_s, the joint PDF for ρ (radial direction) and φ (angular direction) develops as [8, 11]

$$p_{R,F}(\rho,\varphi|c_k,\gamma_s)=\frac{\gamma_s\rho}{\pi}e^{-\gamma_s(\rho^2-2\rho|c_k|\cos\varphi+|c_k|^2)} \tag{15}$$

Therefore,

$$\begin{aligned} q(m,\mu|c_k,\gamma_s) &= E[\rho_k^{\mu}\cos(m\varphi_k)] \\ &= \int_0^{\infty}\int_{-\pi}^{\pi}\rho^{\mu}\cos(m\varphi)\,p_{R,F}(\rho,\varphi|c_k,\gamma_s)d\varphi\,d\rho \end{aligned} \tag{16}$$

The integration over φ provides $I_m(2\rho|c_k|\gamma_s)$, where $I_m(\cdot)$ denotes the mth order modified Bessel function of the first kind [12]. Finally, after some algebraic manipulations, the integration over ρ yields [13]

$$\begin{aligned} &q(m,\mu|c_k,\gamma_s) \\ &\quad= 2|c_k|^{2+\mu}\gamma_s\int_0^{\infty}\rho^{\mu+1}e^{-|c_k|^2\gamma_s(\rho^2+1)}I_m\left(2|c_k|^2\rho\gamma_s\right)d\rho \\ &\quad= |c_k|^m\frac{\Gamma\left(1+\frac{m+\mu}{2}\right)}{\Gamma(1+m)}\gamma_s^{(m-\mu)/2}e^{-|c_k|^2\gamma_s} \\ &\qquad\times\Phi\left(1+\frac{m+\mu}{2},\,1+m,\,|c_k|^2\gamma_s\right) \end{aligned} \tag{17}$$

$\Gamma(\cdot)$ symbolises the Gamma function and $\Phi(a,b,z)$ is the confluent-hypergeometric function, frequently also written as $M(a,b,z)$ or ${}_1F_1(a,b,z)$. Since (15) is an even function of φ, it is easily verified that $E[\rho_k^{\mu}\sin(m\varphi_k)]=0$. Hence, the average over an M-ary signal constellation C with i.i.d. symbols c_k is simply computed as

$$\begin{aligned} Q(m,\mu,\gamma_s) &= E[\rho_k^{\mu}\cos(m\varphi_k+m\delta_k)] \\ &= \frac{1}{M}\sum_{c_k\in C}q(m,\mu|c_k,\gamma_s)\cos(m\delta_k) \end{aligned} \tag{18}$$

where $\delta_k=\arg(c_k)$. For M-PSK schemes with $m=M$, $\cos(m\delta_k)=1$ such that (18) reduces to $Q(m,\mu,\gamma_s)=q(m,\mu|c_k,\gamma_s)$ evaluated at $|c_k|=1$. Finally, if $\gamma_s\gg1$, $\cos(M\varphi_k)\approx1-\frac{1}{2}(M\varphi_k)^2$ and $\rho_k\approx1$ for M-PSK; in this case, (15) is approximately given by $p_F(\varphi|\gamma_s)\approx(\gamma_s/\pi)^{1/2}e^{-\gamma_s\varphi^2}$ and (18) develops as

$$Q(M,\mu,\gamma_s)\approx\sqrt{\gamma_s/\pi}\int_{-\infty}^{\infty}\left[1-\frac{1}{2}(M\varphi)^2\right]e^{-\gamma_s\varphi^2}d\varphi=1-\frac{M^2}{4\gamma_s} \tag{19}$$